Atomistic-model study of temperature-dependent domain walls in the neodymium permanent magnet $Nd_2Fe_{14}B$

Masamichi Nishino,[1,2,*] Yuta Toga,[2] Seiji Miyashita,[3,2] Hisazumi Akai,[4] Akimasa Sakuma,[5] and Satoshi Hirosawa[2]

[1]*International Center for Materials Nanoarchitectonics, National Institute for Materials Science, Tsukuba, Ibaraki, Japan*

[2]*Elements Strategy Initiative Center for Magnetic Materials, National Institute for Materials Science, Tsukuba, Ibaraki, Japan*

[3]*Department of Physics, Graduate School of Science, The University of Tokyo, Bunkyo-Ku, Tokyo, Japan*

[4]*Institute for Solid State Physics, the University of Tokyo, Kashiwanoha 5-1-5, Kashiwa, Chiba, Japan*

[5]*Department of Applied Physics, Tohoku University, Sendai, Japan*

(Received 30 December 2016; revised manuscript received 6 March 2017; published 28 March 2017)

We studied the properties of domain walls (DWs) of the Neodymium magnet, $Nd_2Fe_{14}B$. Applying an atomistic model, in which the magnetic moments of all atoms and exchange interactions were determined by a first-principles calculation (Korringa-Kohn-Rostoker Green's function method), we performed a Monte Carlo simulation for two types of DW, i.e., moving along the *a* axis and along the *c* axis, which are classified into a Bloch-type wall and a Neel-type wall, respectively. We found that the shapes of the DWs of both types are described well by those derived from the continuum model used in micromagnetics. We show that the estimated DW widths are very close to the experimentally evaluated ones. Furthermore, we discovered that the width of the latter type is smaller than that of the former type. We also investigated the temperature dependence of the DW width and found that at higher temperatures it becomes larger and the magnitude of the magnetization becomes smaller, which agrees with experimental observations.

DOI: 10.1103/PhysRevB.95.094429

I. INTRODUCTION

Neodymium magnets [1,2] Nd-Fe-B (Fig. 1), which have high coercive force, are the strongest permanent magnets. They have drawn much attention, especially for their wide commercial usage to electric motors, electronic devices, generators with high efficiency, etc. Intensive studies towards realization of stronger coercive force at higher temperatures are being performed [3,4].

However, the origin of its strong coercive force has not been clarified. To capture it, the mechanisms of nucleation and depinning are key issues [5–8]. The property of magnetic domain walls (DWs), accompanied by nucleation, depinning, or defect, is an important ingredient to be studied.

The DW width is expressed as $\delta W = \pi\sqrt{\frac{A}{K_1}}$ in the continuum model analysis [6], where A is the exchange stiffness constant and K_1 is the magnetocrystalline anisotropy. Temperature dependence of K_1 for $Nd_2Fe_{14}B$ has been reported, based on analysis of magnetization curves along the hard direction [6,9–13]. K_1 has a maximum at around 250 K and reduces with increasing (decreasing) temperature. It becomes negative below the spin reorientation temperature $T_r = 133$–150 K in the bulk [10,12,14–17]. The higher-order term, K_2 rapidly fades away above around 200 K with increasing temperature, and the equation $\delta W = \pi\sqrt{\frac{A}{K_1}}$ is valid at temperatures $T \gtrsim 200$ K.

Empirical evaluation of A is not trivial, but Ono *et al.* evaluated $A = 6.6 \pm 0.3$ pJ/m [18] from spin-wave dispersion curves obtained by neutron-scattering measurements [19,20], assuming $K_1 = 4.5\mathrm{MJ/m^3}$ at room temperature. Other (indirect) methods have given $A = 7.3$–12.5 pJ/m [6,21]. The DW width evaluated from these values of A and K_1 is around 3.6–5.4 nm at room temperature.

Direct observations of the DW have been performed using electron microscopy, and the width has been estimated to be 1–10 nm in the analysis of Lorentz images and electron holography (9 and 10 nm) [22], energy filtered Fresnel images (2 ± 1 nm) [23], and coherent electron shadow images (4 ± 2 nm) [24].

On the other hand, so far the properties of magnetic DWs of the Neodymium magnet including the temperature dependence of the DW width have not been studied from the atomistic theoretical viewpoint. In the present paper, we study the properties of DWs of $Nd_2Fe_{14}B$ with an atomistic-model approach.

Atomistic model studies for other materials, e.g., FePt have been performed [25–28] and various quantitative properties of magnetization process, DWs, etc. have been clarified. Very recently the temperature dependence of magnetic properties of $Nd_2Fe_{14}B$ has been studied with an atomistic Hamiltonian, and relevant bulk properties were given, including the successful reproduction of the reorientation transition [29]. In the atomistic model, the parameters for all atoms and exchange interactions were obtained by a first-principles calculation based on the Korringa-Kohn-Rostoker (KKR) Green's function method. For the anisotropy terms, the values of D_i in Eq. (1) for Fe atoms (six kinds) estimated in a first-principles study [30] were adopted, and experimentally determined A_l^m in Eq. (1) for Nd atoms (2 kinds) [31] were used with $\langle r^l \rangle$ estimated in Ref. [32] because the estimation of A_l^m by first-principles calculations has not been established.

In the present work, we study the properties of DWs of $Nd_2Fe_{14}B$ by a Monte Carlo simulation using the atomic model with the same parameters. The DW nature depends on its moving direction and the two types are investigated: moving along the *a* axis (type I) and along the *c* axis (type

*Corresponding author: nishino.masamichi@nims.go.jp

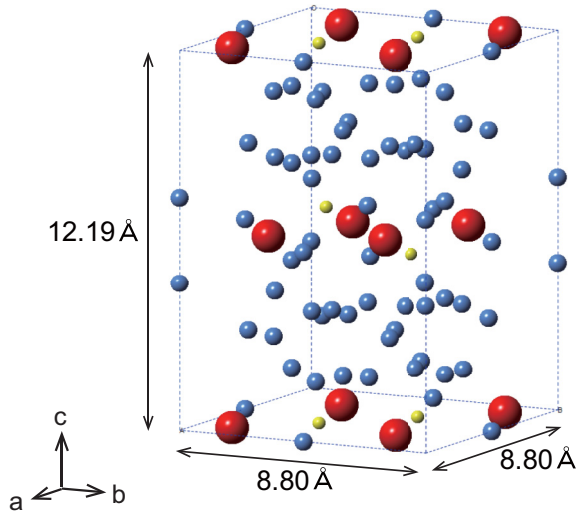

FIG. 1. Unit cell of $Nd_2Fe_{14}B$ magnet, which consists of 68 atoms. Red, blue, and yellow balls denote Nd, Fe, and B atoms, respectively.

II) [Figs. 2(a) and 2(b)]. In the former the plane of the spin rotation is perpendicular to the a axis and we call it Bloch-type wall, while in the latter it includes the c axis and the way of ration is like a Neel wall, and thus we call it Neel-type wall. We find that the shape of DWs obtained by the MC simulation is well fitted by the function derived from the continuum model, and we successfully estimate δW in the atomistic model. It is worth noting that the results in this microscopic study are surprisingly close to the above-mentioned experimental results. We also find a difference in the width between the two types. We demonstrate the increase of the DW width with increasing temperature for both types of DWs, which is consistent with the temperature dependence of K_1 in the experiments.

The rest of the paper is organized as follows. In Sec. II, the model and method are presented. In Sec. III A, the bulk property is shown. In Sec. III B the properties of DW at 300 K are studied and the temperature dependence of the DW width

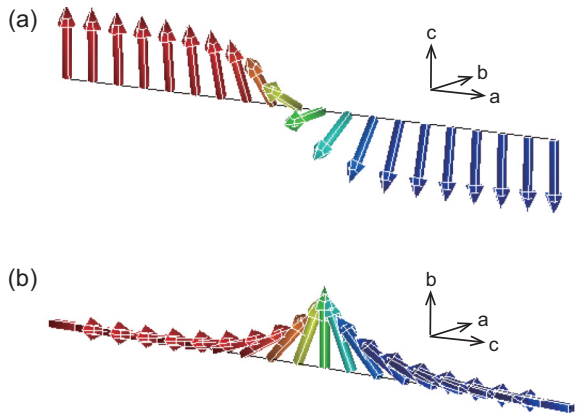

FIG. 2. (a) DW moving along the a axis (type I, Bloch-type wall); (b) DW moving along the c axis (type II, Neel-type wall).

is given in Sec. III C. Section IV is devoted to discussion and summary.

II. MODEL AND METHOD

The $Nd_2Fe_{14}B$ magnet is built up with the tetragonal unit cells (Fig. 1). The experimental values [33] of lattice constants in the a, b, and c axes are $d_a = 8.80$ Å, $d_b = 8.80$ Å, and $d_c = 12.19$ Å, respectively. For the magnet we adopt an atomistic Hamiltonian,

$$\mathcal{H} = -\sum_{i<j} 2J_{ij}\boldsymbol{s}_i \cdot \boldsymbol{s}_j - \sum_{i}^{\mathrm{Fe}} D_i \left(s_i^z\right)^2 + \sum_{i}^{\mathrm{Nd}} \sum_{l,m} \Theta_{l,i} A_{l,i}^m \langle r^l \rangle_i \hat{O}_{l,i}^m, \quad (1)$$

where the first term is the Heisenberg exchange couplings between the ith site and jth site (Nd, Fe, B atoms), D_i denotes the magnetic anisotropy constant of Fe atoms, and the last term is the magnetic anisotropy energy of Nd atoms. Here $\Theta_{l,i}$, $A_{l,i}^m$, $\langle r^l \rangle_i$, and $\hat{O}_{l,i}^m$ are the Stevens factor, the coefficient of the spherical harmonics of the crystalline electric field, the average of r^l over the radial wave function, and the Stevens operator, respectively, at site i for Nd atoms. The summation as to l runs $l = 2,4,6$ and, for simplicity, only diagonal operators $m = 0$ are taken into account. The magnetic moment ($\boldsymbol{S}_i$) of each Nd atom is given by the summation of the moment ($\boldsymbol{s}_i$) of the valence ($5d$ and $6s$) electrons and that ($\boldsymbol{\mathcal{J}}_i$) of the $4f$ electrons: $\boldsymbol{S}_i = \boldsymbol{s}_i + \boldsymbol{\mathcal{J}}_i$.

Here $\mathcal{J}_i = g_{\mathrm{T}} J \mu_{\mathrm{B}}$, where $g_{\mathrm{T}} = 8/11$ is Landé g factor and $J = 9/2$ is the magnitude of the total angular momentum and the directions of $\boldsymbol{s}_i$ and $\boldsymbol{\mathcal{J}}_i$ are antiparallel. It should be noted that d electrons of the Fe atom and $4f$ electrons of the Nd atom do not interact and only $\boldsymbol{s}_i$ contributes to the exchange interaction. For Fe and B atoms, we give $\boldsymbol{S}_i$ the same meaning as $\boldsymbol{s}_i$; i.e., $\boldsymbol{S}_i = \boldsymbol{s}_i$.

We adopt the highly accurate parameter values [29] for the magnetic moments of all atoms and the magnetic interactions, (J_{ij}), obtained by a first-principles computation based on the KKR Green's function method [34]. Since the method does not use any finite basis set, it is free from the serious drawback which originates from using a finite basis set when constructing Green's functions. In addition, the method is an all-electron approach, which guarantees the high reliability [35]. We use the exchange interactions within the range of $r = 3.52$ Å, in which dominant short-range interactions are included. The values for the anisotropy terms are taken from Refs. [30–32], as mentioned in Sec. I.

In this work we use systems of $N_a \times N_b \times N_c$ unit cells with open boundary conditions, where N_a, N_b, and N_c are the number of unit cells in the a, b, and c axes, respectively. For types I and II, $N_a = 32$, $N_b = 5$, $N_c = 5$ and $N_a = 5$, $N_b = 5$, $N_c = 32$ are set, respectively. Each unit cell is referred to by its coordinate (i_a, i_b, i_c).

To realize a DW in each system, the following conditions are imposed: the up-spin state and the down-spin state are fixed at the left-edge cells and the right-edge cells, respectively. In

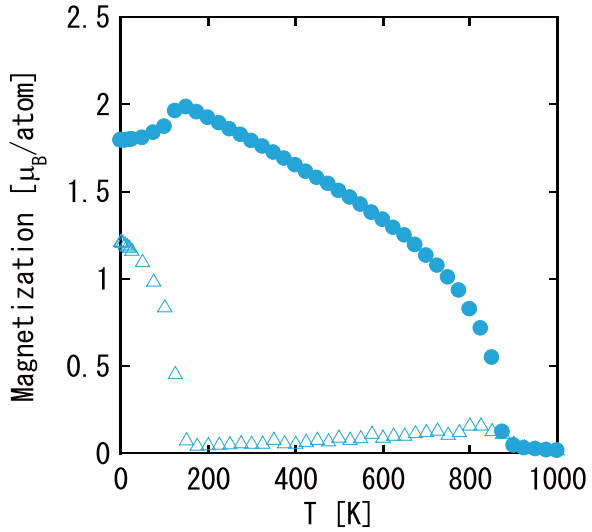

FIG. 3. Temperature dependence of $\tilde{M}_z$ (closed circles) and $\tilde{M}_{xy}$ (open triangles) in the bulk.

type I (II) the left-edge cells are the cells at $i_a = 1$ ($i_c = 1$), and the right-edge cells are the cells at $i_a = 32$ ($i_c = 32$).

III. RESULTS

A. Bulk properties

First we simulate the magnetization in the uniform bulk system ($N_a = 32$, $N_b = 5$, $N_c = 5$) with periodic boundary conditions for reference. In Fig. 3 we plot the temperature dependence of the bulk magnetization $\tilde{M}_z = \frac{1}{N}\sum_i \langle |S_i^z| \rangle$ and $\tilde{M}_{xy} = \langle \sqrt{(\frac{1}{N}\sum_i S_i^x)^2 + (\frac{1}{N}\sum_i S_i^y)^2} \rangle$. Here the summation runs over all the sites and N is the number of total sites and $\langle \cdots \rangle$ denotes thermal average. To obtain the MC data, 400 000 Monte Carlo steps (MCS) were applied for the measurement after the equilibration process of 400 000 MCS. We find that the spin reorientation transition occurs around $T_r = 150$ K, at which $\tilde{M}_z$ has a maximum value. It is close to the experimental values $T_r = 133$–150 K and agrees with the previous work [29]. The feature of the bulk property shows the validity of our modeling [37].

B. Domain wall

Now, we investigate the domain-wall properties. Our strategy to obtain the domain-wall profile is as follows. To study position-dependent magnetization along the a axis and the c axis, we define the z component of the local magnetization,

$$M_z(x) = \frac{1}{N_x}\sum_j S_j^z, \tag{2}$$

where $x/d_a = i_a$ for type I and $x/d_c = i_c$ for type II. Here site index j runs over the spins in the unit cells at i_a for type I and at i_c for type II. N_x is the number of the sites in the unit cells at i_a and i_c for types I and II, respectively. In the same manner the x component $M_x(x)$ and the y component $M_y(x)$ are defined. We also define the amplitude of xy components

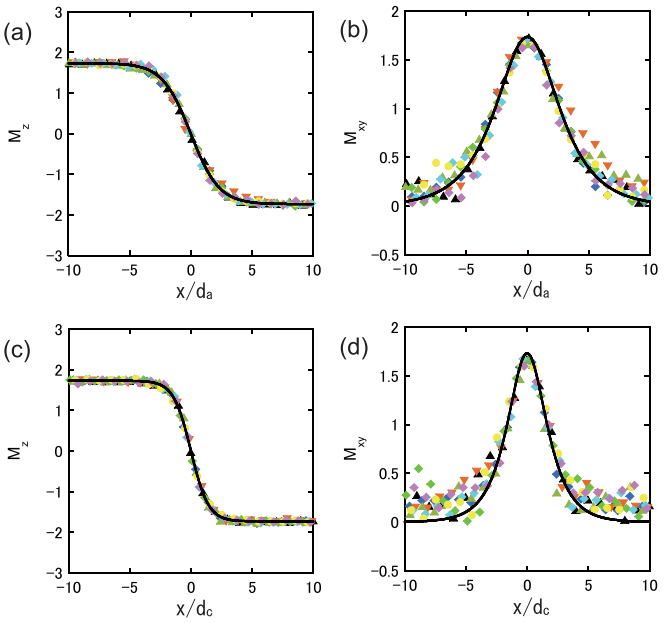

FIG. 4. (a) M_z along the a axis (type I) at 300 K. The unit of the vertical axis is μ_B/atom. (b) M_{xy} along the a axis (type I) at 300 K. (c) M_z along the c axis (type II) at 300 K. (d) M_{xy} along the c axis (type II) at 300 K. The analytical functions $m_z(x)$ and $m_y(x)$ are given by black lines in (a) and (b) [(c) and (d)], respectively. Here symbols denote $M_z(x)$ [M_{xy}] at different MCS.

as

$$M_{xy}(x) = \sqrt{M_x(x)^2 + M_y(x)^2}. \tag{3}$$

We take snapshots of $\{M_z(x)\}$ at given MCS in the equilibrium state. Then the snapshots are fitted by a position-dependent function $m_z(x) = m(T)\cos\theta(x)$, in which $\theta(x)$ is the rotation angle of the spin at x and $m(T)$ is the spin length at temperature T. Applying the relation $\cos\theta(x) = -\tanh(\frac{x}{\delta_0})$, which holds in the continuum model [6], we have

$$m_z(x) = -m(T)\tanh\left(\frac{x}{\delta_0}\right), \tag{4}$$

$$m_y(x) = m(T)\cosh^{-1}\left(\frac{x}{\delta_0}\right), \tag{5}$$

and $m_x(x) = 0$. Here δ_0 is the wall parameter: $\delta_0 \equiv \sqrt{\frac{A}{K_1}}$ and the width of the DW is given by $\delta W = \pi(\frac{dx}{d\theta})_{\theta=\pi/2} = \pi\delta_0 d_X$ ($X = a$ or c).

We fit $m_z(x)$ [Eq. (4)] to the data of snapshots of (2) obtained by the MC method. Here we take δ_0 and $m(T)$ as fitting parameters, and from the fitted values we have δW. Snapshots of M_z along the a axis obtained by the MC method at 300 K are plotted in Fig. 4(a) by symbols. In the MC procedure, snapshots are taken at every 20 000 MCS after the first 400 000 MCS used for the equilibration. The position of the DW fluctuates along the a axis, and thus we shift the center of the DW (x for $M_z = 0$) to the origin of the horizontal axis ($x = 0$).

We find that the MC data are fitted well by the function (4) with $\delta_0 = 2.308$ and $m(T) = 1.734$, which is given by a

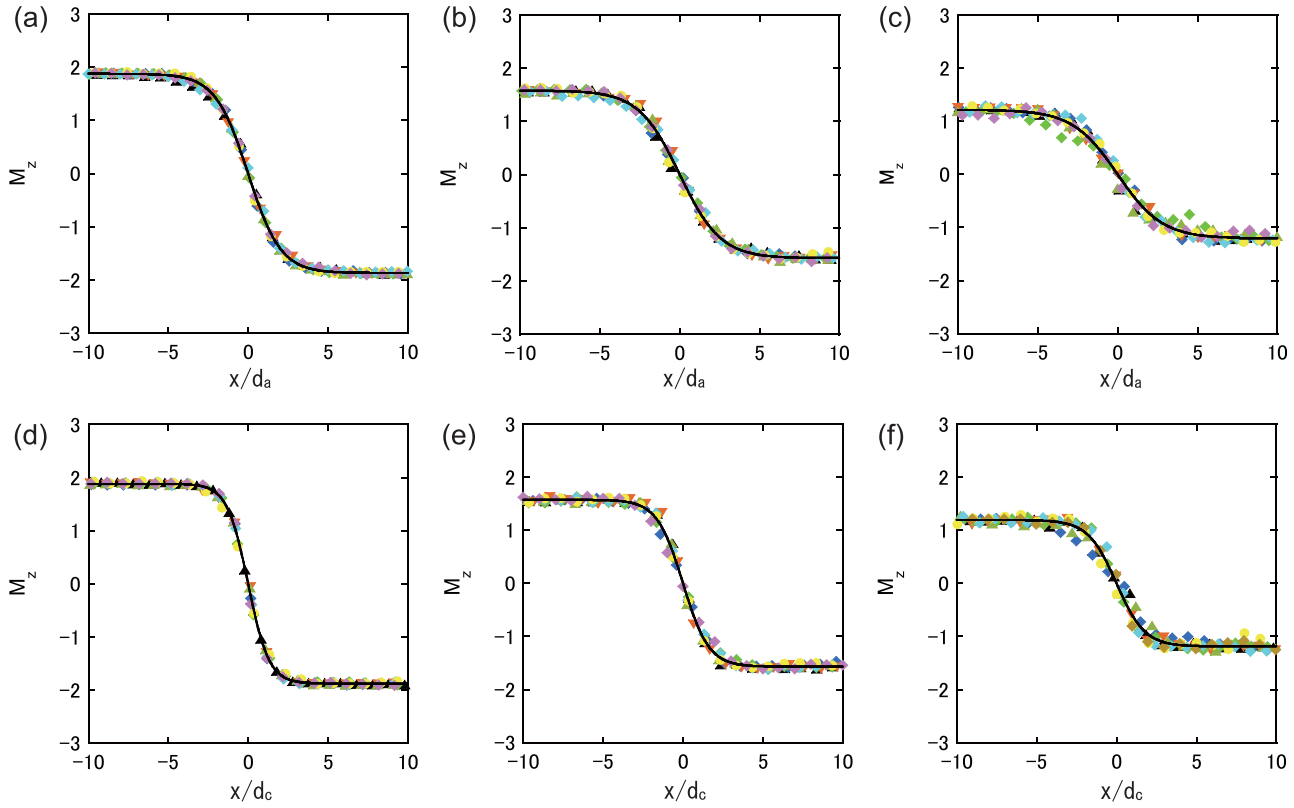

FIG. 5. Temperature dependence of M_z along the a axis (type I) (a)–(c) and along the c axis (type II) (d)–(f). (a),(d) 200 K; (b),(e) 400 K; (c),(f) 600 K. The unit of the vertical axis is μ_B/atom.

black line. Here $\delta W = \pi\delta_0 d_a = 6.38$ nm. Experimental δW at room temperature is 3.6–5.4 nm or 1–10 (see Sec. I), and our estimation is close to the values.

In the figure we do not see the fixed M_z at the edges to focus on only the center part. The edge M_z has a full value of the z component, 2.189 (or -2.189), but M_z decreases (increases) very rapidly within 1–2 unit cells and reaches a saturated value $m(T)$. $m(T)$ is almost the same as $\tilde{M}_z$ in the bulk. This indicates that the fixed magnetizations at the edges do not affect the DW magnetization.

If DW is Bloch-wall type, $m_y(x)$ should be the function (5) and $m_x(x) = 0$ because the profile changes along the x axis. Since the direction of the magnetic anisotropy is parallel to the c axis, the z axis of the spin space and the c axis agree. However, because only exchange interactions (short-range force) are taken into account as magnetic interactions, the direction in the xy plane of the spin space is not determined uniquely; i.e., the x axis and the a axis do not generally coincide. Then, we regard the transverse component M_{xy} as the y component M_y. Snapshots of M_{xy} obtained by the MC method are plotted with symbols in Fig. 4(b).

The function $m_y(x)$ [Eq. (5)] with the fitted parameters $\delta_0 = 2.308$ and $m(T) = 1.734$ is also drawn. We find that the function fits well at relatively large values of M_{xy} by the MC method. Deviation of the MC data from the function is attributed to the definition of M_{xy}, i.e., Eq. (3), in which the squared quantity ($\geqslant 0$) is averaged. We conclude that the DW moving along the a axis is a Bloch wall and the shape is well fitted by the function obtained by the continuum model.

Next we study DWs moving along the c axis (type II). Since the direction of S_z is the same as the c axis and the boundary magnetic moments are parallel to the c axis, the DW is a Neel-type wall. In this case, the same analysis is applied.

We illustrate snapshots of M_z along the c axis with symbols in Fig. 4(c) obtained by the MC method at 300 K. These MC data are well fitted by the function (4) with $\delta_0 = 1.428$ and $m(T) = 1.732$ (black line). Thus, the width is $\delta W = \pi\delta_0 d_c = 5.47$ nm. It is found that the DW width of type II is smaller than that of type I, which is also close to the experimentally estimated values.

Snapshots of M_{xy} obtained by the MC method are plotted with symbols in Fig. 4(d). The function (5) is also given with $\delta_0 = 1.428$ and $m(T) = 1.732$. The MC data are well fitted to the function. The way of spin rotation is different from type I, but the DW shape is similar.

C. Temperature dependence of domain wall

Next we study the temperature dependence of the DW properties. We investigate 200 K and temperatures higher than 200 K. Temperature dependence of the magnetization profile along the a axis (type I) is depicted in Figs. 5 at (a) $T = 200$ K, (b) $T = 400$ K, and (c) $T = 600$ K. We also give function (4) (black line) with $(\delta_0, m(T)) = (2.050, 1.872), (2.572, 1.575)$, and $(2.813, 1.211)$ for Figs. 5(a)–5(c), respectively. Each function fits well to each MC data. Thus, we have $\delta W = 5.67$, 7.11, and 7.78 nm at 200 K, 400 K, and 600 K, respectively. The DW width becomes larger as the temperature increases,

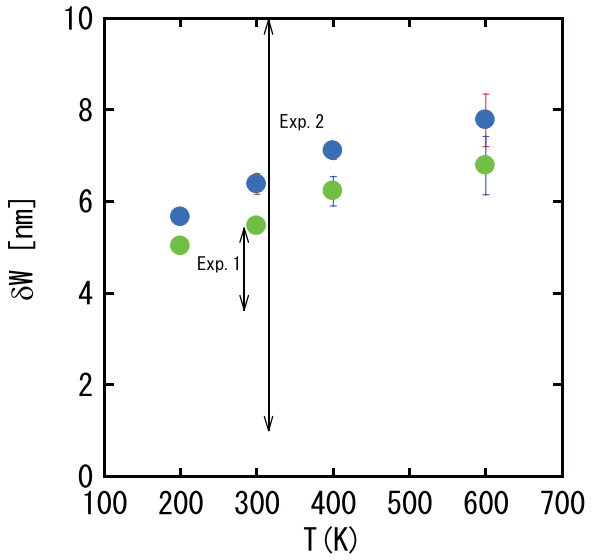

FIG. 6. Temperature dependence of δW in type I (blue circles) and type II (green circles). The up-and-down arrow (Exp. 1) denotes the range of the experimentally estimated δW at room temperature from the values of K_1 and A, and the down arrow (Exp. 2) denotes that obtained by electron microscopes at room temperature.

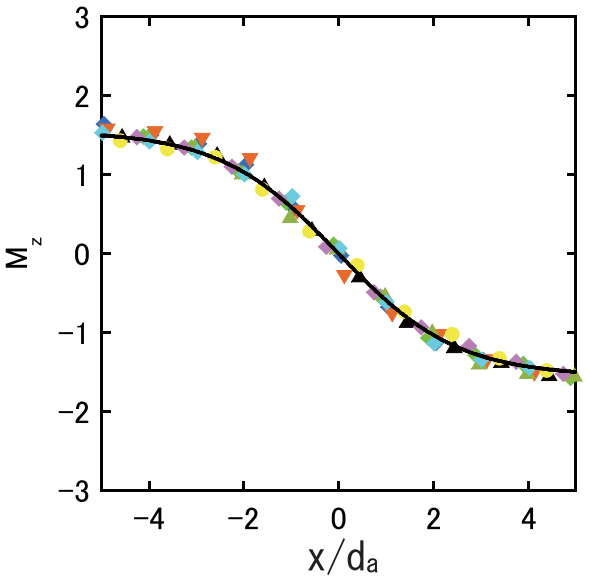

FIG. 7. M_z along the a axis (type I) for the model with the dipole-dipole interaction by the MC method (symbols). The black solid line denotes the function (4) in the text with $\delta = 2.57$ and $m(T) = 1.57$.

which implies that K_1 reduces faster than A with increasing temperature. This is consistent with experimental observations and also a theoretical estimation [29,38].

We also investigate the DW profile for type II. We depict M_z along the c axis with symbols in Figs. 5 at (d) $T = 200$ K, (e) $T = 400$ K, and (f) $T = 600$ K. We give function (4) (black line) with $(\delta_0, m(T)) = (1.313, 1.880), (1.626, 1.571)$, and $(1.772, 1.190)$ for Figs. 5(d)–5(f), respectively. Each function fits well to each MC data. DW widths are $\delta W = 5.03$, 6.23, and 6.79 nm at 200 K, 400 K, and 600 K, respectively. We find the growth of the DW width with the temperature as well as type I. Here the DW widths are smaller than those of the type I.

The temperature dependence of the amplitude $m(T)$ agrees with $\tilde{M}_z$ in the bulk. We checked that the quantitative properties of the DW do not change depending on the system sizes, e.g., $26d_a \times 5d_b \times 5d_c$, etc.

Figure 6 summarizes the temperature dependence of the DW width in our simulation and the range of experimental values at room temperature. The DW widths evaluated by our approach are very close to the experimentally observed values.

IV. DISCUSSION AND SUMMARY

In this study we first gave a microscopic origin to the DW nature for $Nd_2Fe_{14}B$, which has been studied from macroscopic observations so far. The DW of $Nd_2Fe_{14}B$ is well described by the function derived from the continuum model in types I and II. The DW widths for types I and II are different. Orientation dependence of DWs has been pointed out for FePt [25,26], and this property is likely a general characteristic feature of permanent magnet materials where the magnetic parameters themselves are anisotropic, not only the magnetic anisotropy.

The fact that the width for type II is smaller may be attributed to the lattice structure, in which Nd planes are perpendicular to the c axis. In the Nd plane the exchange couplings between neighboring Nd and Fe atoms are small compared to those between neighboring Fe atoms. Namely, exchange energies $|2J_{ij}s_is_j|$ between Fe atoms ($r \leqslant 3.52$ Å) are 16.22–44.6 meV, while those between Nd and Fe atoms are 1.60–7.10 meV. Thus, the correlation across the plane would be smaller.

There have been experimental suggestions [39–41] about the formation of type I walls in the (quasi-)static multidomain state of large grains in $Nd_2Fe_{14}B$, but microscopic structures of DWs are unclear due to technical difficulty. Atomistic-model studies including dynamical aspects will play an important role in elucidation of the condition (environment) for the DW type.

We ignored the dipole-dipole interaction for the model. In the present system sizes, the dipole field applying to each atom is much smaller [$\leqslant O(10^{-3})$] than that from the exchange couplings, and, furthermore, the dipole field from the left of the domain wall and that from the right cancel. We check this estimation. We give in Fig. 7 the domain-wall profile M_z along the a axis (type I) at 400 K by the MC method for the model (1) with the dipole-dipole interaction. The system size is $16d_a \times 5d_b \times 5d_c$. The black solid line denotes the function (4) with $\delta_0 = 2.572$ and $m(T) = 1.575$. We find that the MC data are fitted well by the function. This suggests that the dipole-dipole interaction in such system sizes is negligible for the estimation of the domain-wall width. In larger systems, however, the dipole-dipole interaction may play an important role in the selection of the type of DW in the nucleation process and also the motion of the DW. We will study it in the future.

The properties near the Curie point is interesting from the view point of critical phenomena. For FePt it has been reported that in the temperature region close to the Curie temperature, a linear domain wall dominates the magnetization reversal [42]. In the present paper we concentrated on the domain walls in

a well-ordered state. Study of the possibility of linear DW in $Nd_2Fe_{14}B$ is also interesting from this viewpoint.

The estimation of the DW free energy will be useful because the temperature dependencies of the free energy and the DW width give information about the temperature dependencies of $K(T)$ and $A(T)$, as studied in FePt [43]. The structure of $Nd_2Fe_{14}B$ is more complicated than that of FePt, but the temperature dependence of the DW free energy of $Nd_2Fe_{14}B$ will be a future work.

Coercive force depends on nucleation and domain-wall depinning. In our previous study [8] for a simple model of hard magnetic grains contacting via a soft magnet by using the stochastic Landau-Lifshitz-Gilbert approaches [28,44], nucleation filed and pinning filed depends on A and K_1 and also dynamical effects including thermal fluctuation at finite temperatures. The application of this kind of study to the present atomistic model for $Nd_2Fe_{14}B$ may give us important information about the relation between domain-wall properties and nucleation and pinning fields in $Nd_2Fe_{14}B$, which will be studied in the future.

ACKNOWLEDGMENTS

The present work was supported by Grants-in-Aid for Scientific Research C (Grants No. 26400324 and No. 25400391) from MEXT of Japan, and the Elements Strategy Initiative Center for Magnetic Materials (ESICMM) under the outsourcing project of MEXT. The authors thank the Supercomputer Center, the Institute for Solid State Physics, the The University of Tokyo, for the use of the facilities.

[1] M. Sagawa and S. Hirosawa, J. Mater. Res. **3**, 45 (1988).
[2] J. F. Herbst, Rev. Mod. Phys. **63**, 819 (1991).
[3] H. Sepehri-Amin, T. Ohkubo, S. Nagashima, M. Yano, T. Shoji, A. Kato, T. Schrefl, and K. Hono, Accta Mater. **61**, 6622 (2013).
[4] T. Akiya, J. Liu, H. Sepehri-Amin, T. Ohkubo, K. Hioki, A. Hattoric, and K. Hono, Scr. Mater. **81**, 48 (2014).
[5] K.-D. Durst and H. Kronmüller, J. Magn. Magn. Mater. **68**, 63 (1987).
[6] H. Kronmüllar and M. Fähnle, *Micromagnetism and the Microstructure of Ferromagnetic Solids* (Cambridge University Press, Cambridge, UK, 2003).
[7] A. Sakuma, S. Tanigawa, and M. Tokunaga, J. Magn. Magn. Mater. **84**, 52 (1990).
[8] S. Mohakud, S. Andraus, M. Nishino, A. Sakuma, and S. Miyashita, Phys. Rev. B **94**, 054430 (2016).
[9] S. Hirosawa, Y. Matsuura, H. Yamamoto, S. Fujimura, M. Sagawa, and H. Yamauchi, J. J. Appl. Phys. **24**, L803 (1985).
[10] S. Hirosawa, Y. Matsuura, H. Yamamoto, S. Fujimura, M. Sagawa, and H. Yamauchi, J. Appl. Phys. **59**, 873 (1986).
[11] A. V. Andreev, A. V. Deryagin, N. V. Kudrevatykh, N. V. Mushnikov, V. A. Reimer, and S. V. Terent'ev, Sov. Phys. JETP **63**, 608 (1986).
[12] O. Yamada, Y. Ohtsu, F. Ono, M. Sagawa, and S. Hirosawa, J. Magn. Magn. Mater. **70**, 322 (1987).
[13] N. V. Mushnikov, P. B. Terent'ev, and E. V. Rosenfel'd, Phys. Met. Metallogr. **103**, 39 (2007).
[14] X. Kou *et al.*, Phys. Rev. B **54**, 6421 (1996).
[15] C. Pique *et al.*, J. Magn. Magn. Mater. **154**, 71 (1996).
[16] Z. Zhang *et al.*, J. Alloys Compd. **274**, 274 (1998).
[17] C. Chacon *et al.*, J. Alloys Compd. **283**, 320 (1999).
[18] K. Ono, N. Inami, K. Saito, Y. Takeichi, M. Yano, T. Shoji, A. Manabe, A. Kato, Y. Kaneko, D. Kawana, T. Yokoo, and S. Itoh, J. Appl. Phys. **115**, 17A714 (2014).
[19] H. M. Mayer, M. Steiner, N. Stiller, H. Weinfurter, B. Darner, P. A. Lindgrad, K. N. Clausen, S. Hock, and R. Verhoef, J. Magn. Magn. Mater. **104**, 1295 (1992).
[20] H. M. Mayer, M. Steiner, N. Stußer, H. Weinfurter, K. Kakurai, B. Dorner, P. A. Lindgard, K. N. Clausen, S. Hock, and W. Rodewald, J. Magn. Magn. Mater. **97**, 210 (1991).
[21] M. Sagawa, S. Fujimura, H. Yamamoto, Y. Matsuura, S. Hirosawa, and K. Hiraga, in *Proceedings of the 4th International Symposium on Magnetic Anisotropy and Coercivity in Rare Earth Transition Metal Alloys*, edited by K. J. Strnat (University of Dayton, Dayton, OH, 1985), p. 587.
[22] Y. Zhu and M. R. McCartney, J. Appl. Phys. **84**, 3267 (1998).
[23] S. J. Lloyd, J. C. Loudon, and P. A. Midgley, J. Microsc. **207**, 118 (2002).
[24] M. Beleggia, M. A. Schofield, Y. Zhu, and G. Pozzi, J. Magn. Magn. Mater. **310**, 2696 (2007).
[25] D. Hinzke, U. Nowak, R. W. Chantrell, and O. N. Mryasov, Appl. Phys. Lett. **90**, 082507 (2007).
[26] D. Hinzke, N. Kazantseva, U. Nowak, O. N. Mryasov, P. Asselin, and R. W. Chantrell, Phys. Rev. B **77**, 094407 (2008).
[27] T. A. Ostler, R. F. L. Evans, R. W. Chantrell, U. Atxitia, O. Chubykalo-Fesenko, I. Radu, R. Abrudan, F. Radu, A. Tsukamoto, A. Itoh, A. Kirilyuk, T. Rasing, and A. Kimel, Phys. Rev. B **84**, 024407 (2011).
[28] R. F. L. Evans, W. J. Fan, P. Chureemart, T. A. Ostler, M. O. A. Ellis, and R. W. Chantrell, J. Phys.: Condens. Matter **26**, 103202 (2014).
[29] Y. Toga, M. Matsumoto, S. Miyashita, H. Akai, S. Doi, T. Miyake, and A. Sakuma, Phys. Rev. B **94**, 174433 (2016).
[30] Y. Miura, H. Tsuchiura, and T. Yoshioka, J. Appl. Phys. **115**, 17A765 (2014).
[31] M. Yamada, H. Kato, H. Yamamoto, and Y. Nakagawa, Phys. Rev. B **38**, 620 (1988).
[32] A. J. Freeman and R. E. Watson, Phys. Rev. **127**, 2058 (1962).
[33] J. F. Herbst, J. J. Croat, F. E. Pinkerton, and W. B. Yelon, Phys. Rev. B **29**, 4176 (1984).
[34] A. I. Liechtenstein, M. I. Katsnelson, V. P. Antropov, and V. A. Gubanov, J. Magn. Magn. Mater. **67**, 65 (1987).
[35] We used the local density approximation (LDA) of the density functional theory with the parametrization given by Morruzi, Janak, and Williams [36]. The $4f$ states rare-earth atoms were treated as open cores; the self-interaction correction was exploited for these states. We first performed the self-consistent LDA calculation using 4 k points within the irreducible wedge of Brillouin zone. Then the number of k points was increased up to 32 to calculate J_{ij}'s for this self-consistent potential.

[36] V. L. Morruzi, J. F. Janak, and A. R. Williams, *Calculated Electronic Properties of Metals* (Pergamon, New York, 1978).

[37] The critical temperature ($T_c \sim 800$ K) (Fig. 3) is slightly larger than the experimental values [10,11] $T_c \sim 600$–700 K, and the difference may be due to a small amount of overestimation of magnetic interactions. If we consider this difference, the correction of the width evaluated in the present study is at most 12% assuming $A \propto T_c$.

[38] R. Sasaki, D. Miura, and A. Sakuma, Appl. Phys. Express **8**, 043004 (2015).

[39] H. S. Park, Y.-G. Park, Y. Gao, and D. Shindo, J. Appl. Phys. **97**, 033908 (2005).

[40] S. Yamamoto, M. Yonemura, T. Wakita, K. Fukumoto, T. Nakamura, T. Kinoshita, Y. Watanabe, F. Z. Guo, M. Sato, T. Terai and T. Kakeshita, Mater. Trans. **49**, 2354 (2008).

[41] Y. Murakami, T. Tanigaki, T. T. Sasaki, Y. Takeno, H. S. Park, T. Matsuda, T. Ohkubo, K. Hono, and D. Shindo, Acta Mater. **71**, 370 (2014).

[42] J. Barker, R. F. L. Evans, R. W. Chantrell, D. Hinzke, and U. Nowak, Appl. Phys. Lett. **97**, 192504 (2010).

[43] U. Atxitia, D. Hinzke, O. Chubykalo-Fesenko, U. Nowak, H. Kachkachi, O. N. Mryasov, R. F. Evans, and R. W. Chantrell, Phys. Rev. B **82**, 134440 (2010).

[44] M. Nishino and S. Miyashita, Phys. Rev. B **91**, 134411 (2015).